XVII IAHR SYMPOSIUM
Beijing, China 1994

ACCELEROMETER AND PIT COUNTING DETECTION OF CAVITATION EROSION ON A LABORATORY JET AND A LARGE FRANCIS TURBINE

BOURDON, Paul — Hydro-Québec, IREQ — Canada
SIMONEAU, Raynald — Hydro-Québec, IREQ — Canada
DOREY, Jean-Marc — Électricité de France, DER-Chatou — France

ABSTRACT

The two techniques, vibratory monitoring and pit counting, show promising results for the prediction of prototype cavitation erosion from model tests of Francis turbines. These cavitation detection methods are compared in two set-ups at different power levels, a laboratory high velocity cavitation jet and a full scale 270 MW Francis turbine. Excellent quantitative correlations are obtained in the jet tests between erosion rate, volume pitting rate measured on polished metal surfaces of different hardness with a laser profilometer and the mean square value of forces on the eroded specimen inferred from measurements with a high frequency accelerometer on the specimen holder. On the large prototype good coherent results are also obtained but the vibratory information requires much finer analysis. In particular the varying erosive cavitation intensity with power output level is well detected by both methods. The two cavitation detection techniques exhibit great dynamic range and can prove very useful in characterizing the erosive aggressiveness of cavitating flow both in large machines and in reduced scale models.

RÉSUMÉ

Les deux techniques, la surveillance vibratoire et le comptage d'empreintes, donnent des résultats prometteurs pour la prédiction de l'érosion de cavitation de prototypes à partir d'essais de modèles de turbines Francis. Ces deux méthodes de détection de la cavitation sont comparées dans deux équipements opérés à différentes puissances, un jet de cavitation à haute vitesse en laboratoire et une grande turbine Francis de 270 MW. Les essais au jet donnent d'excellentes corrélations quantitatives entre le taux d'érosion, le taux volumique de marquage mesuré sur des surfaces métalliques polies de dureté variée à l'aide d'un profilomètre au laser et la valeur quadratique moyenne des forces inferrées sur l'échantillon érodé mesurées à l'aide d'un accéléromètre haute fréquence monté sur son support. Les essais sur la grande turbine montrent aussi de bons résultats cohérents mais les données vibratoires demandent une analyse beaucoup plus fine. En particulier l'intensité de la cavitation érosive variant avec la puissance de la machine est bien mise en évidence par les deux techniques. Ces deux méthodes de détection de la cavitation montrent une grande plage dynamique et pourront se montrer très utiles pour caractériser l'agressivité érosive d'un écoulement cavitant à la fois dans les grandes machines et dans les modèles à échelle réduite.

1 INTRODUCTION

To this date, cavitation erosion has remained a problem with Francis turbines, both from a design and an operation point of view[1]. The prediction of prototype cavitation erosion from model tests is also not presently fully reliable. To correct this technically and economically unacceptable state of things, practical and accurate prediction tools must be developed. With this objective in mind, Électricité de France, Hydro-Québec and l'École Polytechnique Fédérale de Lausanne have united their resources in a research project having for objective to develop reliable and accurate tools to assess the potential erosive power of model Francis turbines[2-3].

Two promising tools for this application are cavitation aggressiveness characterization by high frequency accelerometer measurements presently in use at Hydro-Québec in the development of an erosive cavitation monitoring technique on prototypes[4-5-6] and direct pit counting techniques as developed by EDF and other French laboratories[7-8] and used on pumps and valves. This paper presents experimental results obtained on a laboratory jet cavitation apparatus and a prototype Francis turbine using both approaches.

2 LABORATORY CAVITATION JET PROGRAM

2.1 Objectives

Recent investigations by Simoneau et al. have shown that the high pressure jet cavitation apparatus appears to better reproduce the stronger cavitation impacts seen by large hydroturbines[9-10]. This conclusion stems mostly from the similar pit diameters and depths observed on samples exposed to high intensity jet cavitation as compared to those left on the various parts of prototype runners by cavitating flow. In this research program it was decided to compare pit marks produced in the high pressure cavitating jet on polished samples of metals to those produced by actual cavitating flows on polished 316L stainless steel disks imbedded flush in the low pressure profile of a Francis runner blade. In both set-ups vibratory cavitation measurements would also be performed with high frequency accelerometers and measured transmissibility functions. This would allow to infer acting forces on the samples or runner blades and to assess the merits of this vibratory approach in evaluating the aggressiveness of turbine cavitation as indicated by the pitted state of the samples.

2.2 The high pressure cavitating jet

The mechanical layout of the jet system is shown in Figure 1. A high pressure water pump can deliver water at up to 42 MPa (6000 p.s.i.) to a small diameter sapphire nozzle (0.5 to 1 mm) which accelerates it to velocities reaching 300 m/sec. The nozzle outlet has been cone shaped to increase further the cavitation intensity. The external enclosure is made of stainless steel that can sustain pressures up to 1000 kPa. Both the pump high pressure and the reservoir low pressure are controlled by mechanical valves and pressure gauges. Water is recirculated with the addition of tap water as necessary to control pressure and temperature. The test specimen is held at a constant 17 mm distance from the nozzle outlet on a rotary holder. At the high velocity of the water at the nozzle outlet, the local water pressure drops below the vapor pressure producing violent vaporization and cavitation. The water jet hits the specimen surface and decelerates and the pressure surge produces very intense collapses of the cavities at the specimen surface. The rocket effect (conservation of kinetic momentum) of the traveling bubbles energizes greatly the impacts. For the pit counting experiments, the specimen were rotated in the support for short periods of time of 0.03 and 0.15 second by the drive shaft at 150 and 30 rpm respectively. This submitted the specimen surfaces to steady state cavitation.

2.3 Sample preparation and transmissibility measurements

Samples of Al59 aluminum, 316L stainless steel and 440c stainless steel were prepared in metallographic resin and mechanically fine polished down to 0.05 μm mean roughness. Before

running the tests, the transmissibility function expressing the ratio of the output acceleration autospectrum at the monitoring point to the input force autospectrum was measured on each of the samples mounted in the rotary sample holder. The reservoir was filled with water just flush with the sample upper surface. An instrumented miniature Dytran 5800SL force hammer was utilized to apply 16 impacts on the exposed area of the sample and both the force impacts and the acceleration response of a Kistler 8616A1000 accelerometer mounted on the flange coupling of the rotating drive shaft of the specimen support assembly (see Figure 1) was recorded on a HP 3562A 2 channel spectrum analyzer. The averaged transmissibility function in Figure 2 for 316L stainless steel is shown with its coherence function with the solid lines. This last function implies that the measured transmissibility is usable to 25 and even 30 kHz with confidence. For a 16 average measurement, the transmissibility function should have for value at each frequency the value shown +/- ≈ 3.5 dB 9 times out of ten. The transmissibility for Al59 is shown in dashed lines on the graph. For the 440C the curve was very similar to the one for the 316L. The transmissibility functions thus measured were utilized to infer the acting forces on the samples by dividing the acceleration autospectrum recorded at the monitoring point under test conditions by the appropriate transmissibility function.

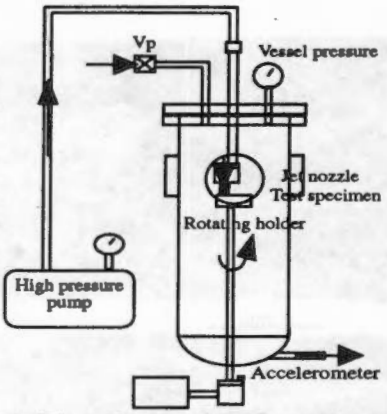

Fig. 1. Schematic view of IREQ cavitation jet.

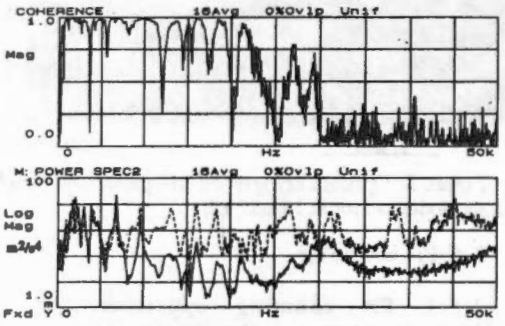

Figure 2. Transmissibility function measured on the jet apparatus for 316l and Al59 specimens.

2.4 Jet test conditions.

The four test conditions that were utilized in the jet tests are described in Table 1. The erosion rate of Al6061T6 serves as a calibration of the erosive intensity of the jet under the four retained conditions

Table 1 Jet test parameters

Test I.D.	High pressure	Chamber pressure	Al6061T6 eros. rate
	(MPa)	(kPa)	(mg/h)
7	6.9	169	36.8
14	13.8	238	126
21	20.7	376	583
34	34.5	513	1489

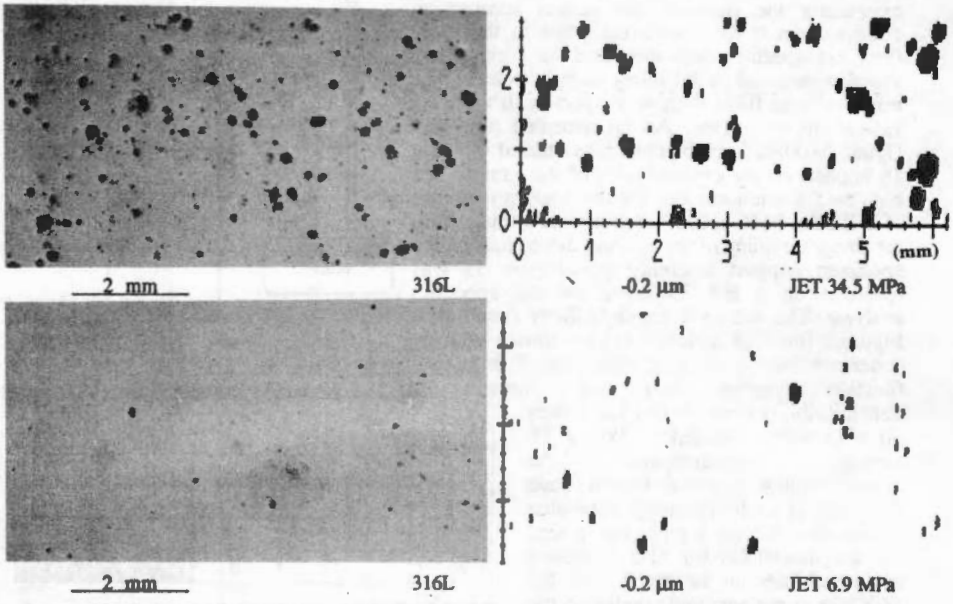

Figure 3. Optical micrographs and pitted area profilometer output of 316L surfaces exposed to jet cavitation for 0.15 second.

2.5 Pit counting

2.5.1 Pit counting apparatus. The exposed surfaces of the samples have the following dimension range: width between 12 and 18 mm and length between 12 and 20 mm. The exposure time was adjusted, through the rotation speed of the sample holder, in order to have at least 100 pits within the measured area of 1 cm2 and less than 25% of pitted areas in the scanned area. It was set to 0.15 s for all tests except for the softest metal, Al59, at the highest intensity (35 MPa) for which it was set to 0.03s. The pitted surfaces were analyzed with a 3-D optical laser UBM profilometer. With its x-y scanning sample holder this equipment uses a focused laser spot of 1 µm with a z resolution of 5 nm and a x-y resolution of 0.5 µm. The system software can produce 3-D surface plots or contour lines and calculate the total pit area for a given depth and the total pit volume. All the samples were scanned on an area of 10 by 10 mm at a resolution of 20 points per mm.

2.5.2 Pit counting results. Figure 3 shows optical micrographs and profilometer output taken at a depth of 0.2 µm on the 316L exposed to jet cavitation for 0.15 s at the two extreme jet cavitation intensities. The effect of cavitation intensity is obvious. As can be observed on the

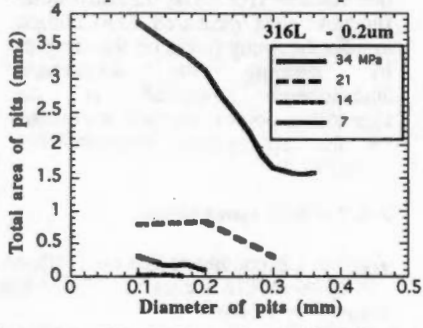

Figure 4. Distribution of pit diameter on 316L at the four jet intensities.

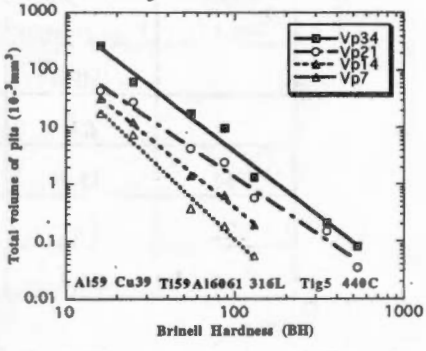

Figure 5. Total pit volume vs hardness for the 4 jet intensities and the 7 alloys.

micrographs of Figure 3 and on the pit diameter distribution of Figure 4, there is a finite number of larger pits characterized by the cavitation intensity such as about 0.2 mm on 316L for the highest intensity. There is also a larger number of smaller pits, of diameter smaller than 0.1 mm. The total number of pits, of the order of a few hundreds for an exposure time of 0.15s corresponds with the characteristic acceleration frequency of a few kHz observed on the high frequency accelerometer signal. In addition to the three materials mentioned above others, spanning a range of Brinell hardness of 16 to 530, were submitted to the jet tests to examine the effect of hardness on cavitation resistance. Figure 5 shows the total volume of pits as calculated from the pitted areas at different depths for all materials and all test conditions. A good correlation is found with the material hardness. The correlation was not as good with either the material yield or tensile strength, which is not surprising since both hardness indentation and cavitation pitting are somehow similar processes, except for the strain rate. These data indicate that the strain rate effect is not very important in these materials. There may be some for 316L which presents lower cavitation pitting than predicted by the correlation curve. An opposite effect seems to be prevalent for Al6061T6 and it could be related to the larger brittleness of this hardened alloy. This pit counting technique is good to measure the aggressiveness or erosive power of cavitation as Figure 6 demonstrates: here the measured steady state (measured after the incubation period) erosion rate of Al6061T6 is taken as a measure of erosive cavitation intensity. The volume pitting rate of the 7 materials of Figure 5 are plotted against the Al6061T6 erosion rate. The correlation is particularly good for Cu39 and 316L that can be used to cover a fairly wide range of cavitation intensity. 316L will be used on this basis for measurements on a Francis prototype turbine which we will describe later in this article.

2.6 Measured acceleration and inferred forces

The pit counting technique above has shown that at higher jet intensity, larger pits are observed along with a greater area of smaller pits. The measured Mean Square Value (MSV) of acceleration measured in the four tests on the three samples are shown in Figure 7 with the corresponding inferred forces. The results are presented in the 0.5 to 11 kHz frequency band where all three transmissibility functions have

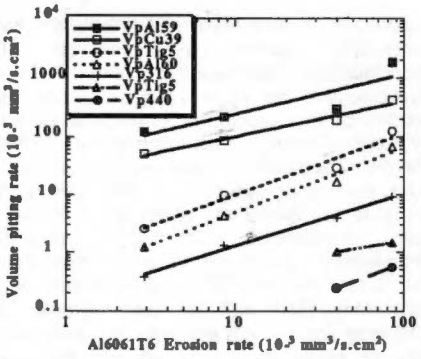

Figure 6. Volume pitting rate vs Al6061T6 erosion rate.

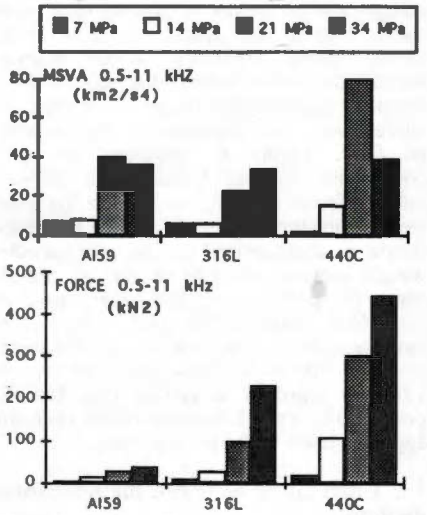

Figure 7. MSV of acceleration and inferred forces for 4 jet intensities and 3 metals of significantly different hardness.

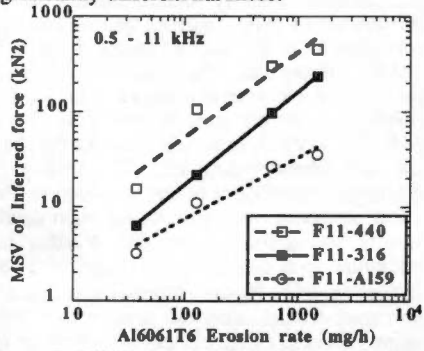

Figure 8. MSV of 0.5-11kHz inferred forces versus jet intensity expressed as Al6061T6 erosion rate.

shown good coherence and where the more significant forces are observed. The accelerations illustrated on Figure 7 do not indicate that the aggressiveness of the tests increases with ascending jet pressure or water velocity. Depending on the material, different levels of acceleration response are recorded at the monitoring point for the various test conditions. However, when these responses are normalized by the measured transmissibility functions, the inferred forces all fall in line with the aggressiveness of the cavitating flow and on each sample, the inferred forces increase with the severity of the cavitation attack. The inferred forces for each test condition are greater on the harder material. This indicates that the cavitation energy is used mostly to produce pits in the softer material and elastic vibration in the harder material. However, for each material, the inferred forces reveal, due account being taken for the individual material properties, the aggressiveness of the attack of the cavitating jet flow. Figure 8 illustrates the good correlations obtained between the MSV of inferred forces in the 0.5 to 11 kHz frequency band for the three materials and the jet erosive power as characterized by the corresponding weight loss erosion rate of the Al 6061T6 alloy. The correlation is particularly good for the 316L ss which will be used for the tests on the prototype. Just as was the case for the pit counting technique described earlier, the vibratory approach as applied here has also proven to be a good describer of the cavitation aggressiveness of the jet apparatus.

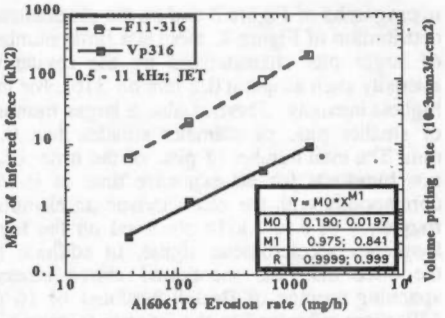

Figure 9. Comparison of the two detection method data, vibratory and pit counting, obtained on 316L samples at the 4 jet intensities.

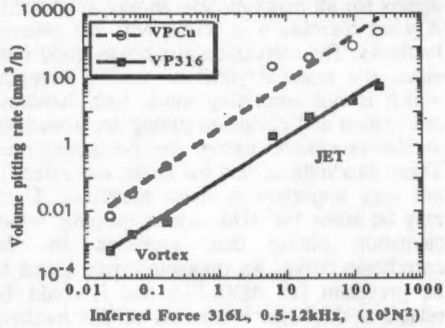

Figure 10. Correlation between inferred force and volume pitting rate of Cu39 and 316L in both jet and vortex cavitation.

2.7 Correlation between the pit counting and vibratory characterization methods

Since the 316L alloy has been selected for the prototype pit counting application which will also include vibratory measurements, the two detection methods applied to this material are compared in Figure 9 against the erosion aggressiveness of the jet as described previously. The top curve plots the inferred forces in the 0.5-11 kHz frequency band and the bottom one, the volume pitting rate. The parallelism of both curves is good, indicating that both detection methods bear similar exponential relations to the erosion rate of Al6061T6. The values of these power relations are listed in the box in the lower right hand corner of the graph. An exponent of 0.975, very close to 1.0 is found for the inferred forces while 0.841, slightly less, applies for the volume pitting rate. The quality of the power law curve fit is described by the correlation coefficient of the fit which is above 0.999 in both cases. These very good results show that these two methods are valid cavitation detection tools when all factors affecting the results are carefully controlled. Further confidence in these two methods is provided by additional tests that were performed in the single vortex cavitation generator at IMHEF-EPFL in Lausanne [3]. Figure 10 presents the jet results for the 316L and Cu39 as well as the vortex generator results using the same two techniques. The volume pitting rates characterizing the aggressiveness of the cavitation in both set-ups are plotted against the MSV of inferred forces. We see that even if the levels of the volume pitting rate and inferred forces are more than two orders of magnitude lower in the vortex than in the jet, good correlations between the volume

pitting rate and the inferred forces are obtained over the complete range. These results underline the excellent dynamic range and consistency of the pit counting and vibratory cavitation intensity characterization methods in the laboratory environment. We will now focus our attention on the prototype investigation program.

3 PROTOTYPE CAVITATION PROGRAM

3.1 Prototype characteristics

In order to test on a prototype the cavitation erosion detection tools described above, an operating Francis turbine with a well documented cavitation erosion history with an intermediate head value and accessible for geometry measurements and pitting tests was chosen. This machine was acceptable to all partners in this joint research effort. The turbine (prototype A), in one of Hydro-Québec's powerplants, has the following characteristics: nominal head, 145 m, nominal power, 240 MW, maximum, 266 MW, nominal discharge, 180 m^3/s with a transposed best efficiency over 95.5%, synchronous speed, 180 r.p.m., normal plant sigma of 0.134 with range of 0.102 to 0.156. The outlet diameter is 4.4 m, there are 13 blades and 20 guide vanes and the distributor height is 1.1 m. The runner is of cast A27 mild steel with welded 308 stainless steel overlays. Repairs have been performed with Stellite 21 and Ireca-Hydroloy.

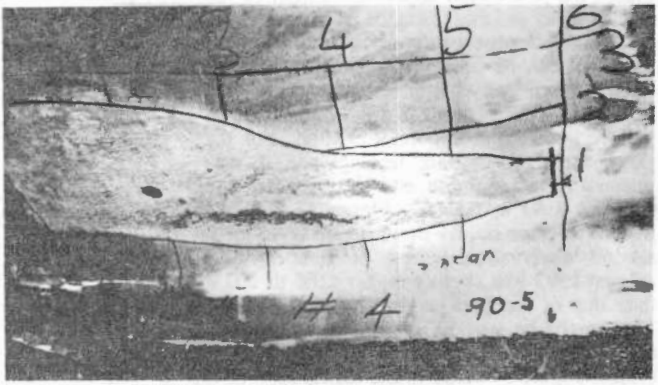

Figure 11. Illustration of erosion on blade 4 of prototype A in 1990.

3.2 Erosion history and patterns

The machine was put into service in 1989 and was first inspected for cavitation damage in 1990 after 4500 hours of operation. As on other units of this prototype, the damages were all located in the same area on the low pressure side of the blades near the trailing edge and the band. Figure 11 shows a typical damage pattern on one of the blades after the first 4500 hour run of the machine. At that time, the evaluated weight loss of 308 ss was close to 14 kg with a maximum penetration rate of 8 mm/a. Repairs were made with Stellite 21 which reduced this rate to ≈ 1 mm/a. This reduction is possibly also attributable to changes in operating conditions because erosion rates were generally

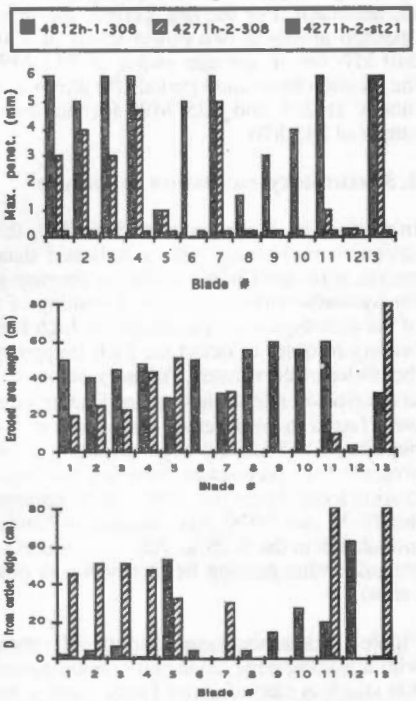

Figure 12. Maximum penetration, length and distance from trailing edge of eroded areas on prototype A after the two operating periods.

reduced by a factor of 5 in going from 308 to Stellite 21 overlays in other powerhouses. Additionally, over the next two years after the repairs up to the second inspection in 1992, not only did the damages diminish in importance, depth and area, but they migrated upstream away from the trailing edge of the blade up the blade to band fillet. Figure 12 shows for all 13 blades the penetration depth, the length of the eroded areas and their distance from the trailing edge for both observation periods. From these graphs it can be seen that blades 5,8 and 12 have shown very little erosion since the beginning while blades 1,2,3,4,11 and 13 have yielded similar and important erosion. For the purposes of the pitting tests, blade 4 was retained as a mounting site for polished 316L stainless steel specimens. Figure 13 illustrates that the average hourly downstream level for the second observation period of June 1990 to August 1992 was slightly higher (205 to 207 m) than that of the first period (204.5 to 206 m). This might be part of the explanation for the upstream migration of the damaged areas on the blades. Figure 14 displays the distribution of the operating hours versus the power generated by the alternator. For the first period, the unit was operated mostly at two power levels of 230 and 240 MW for an average output of 231 MW. In the second observation period, the unit was run mostly at 205 and 225 MW for an average output of 215 MW.

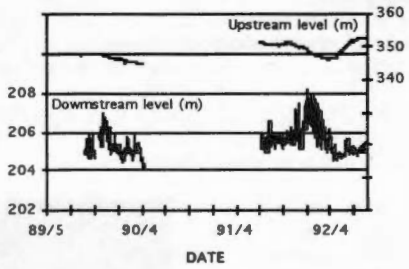

Figure 13. Upstream and downstream level history of powerhouse A.

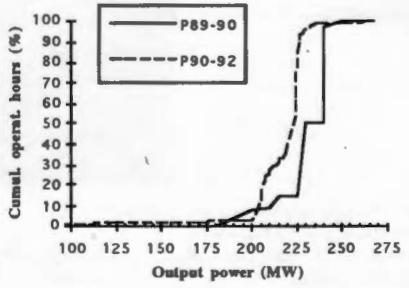

Figure 14. Power output history for the two periods corresponding to damage reports of fig. 12.

3.3 Vibratory cavitation signature

In view of its cavitation erosion history, this machine had been chosen for on line vibratory cavitation monitoring with a dedicated data acquisition system in the course of a research project at Hydro-Québec aiming to develop an effective cavitation erosion monitoring technique for hydraulic turbines. At the beginning of this monitoring program, the cavitation signatures of the prototype were recorded with high frequency accelerometers mounted at the lower guide bearing in order to detect the high frequency vibration generated by the cavitation impacts on the blades of the runner. Vibratory parameters which had been demonstrated to be proportional to the erosion rate in the case of leading edge cavitation[5,11] were recorded. These signatures were found to be different from those of a number of other machines that had been recorded but that all had leading edge cavitation erosion problems. To illustrate this point, Figure 15 presents four parameters recorded for the prototype involved in the pitting tests with the erosion located near the outlet. These parameters are the Mean Square Value of acceleration in the 15-30 and 70-85 kHz frequency bands, the MSV of 70-85 kHz acceleration amplitude modulation in the 0.25 to 100 Hz frequency band and the same parameter but at 60 Hz only, the guide vane passing frequency for an observer rotating with the runner (3 r.p.s., 20 guide vanes).

Figure 16 presents corresponding information for a 200 MW Francis turbine (prototype B) with a leading edge cavitation erosion pattern characterized by a maximum penetration rate in 308 stainless steel of about 3 mm/a with a metal loss rate of 3 kg/a. This machine also has 13 blades and 20 guide vanes but with a guide vane passing frequency of 37.5 Hz (1.875 r.p.s.). The modulation information in Figure 16 is slightly different from that of Figure 15 in that the band of high frequencies is now 28 to 44 kHz and the analysis range 0.25 to 200 Hz. Since

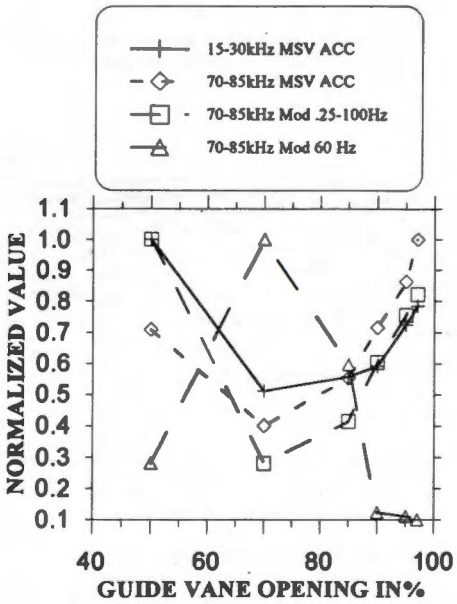

Fig.15. Vibratory cavitation signature of prototype A.

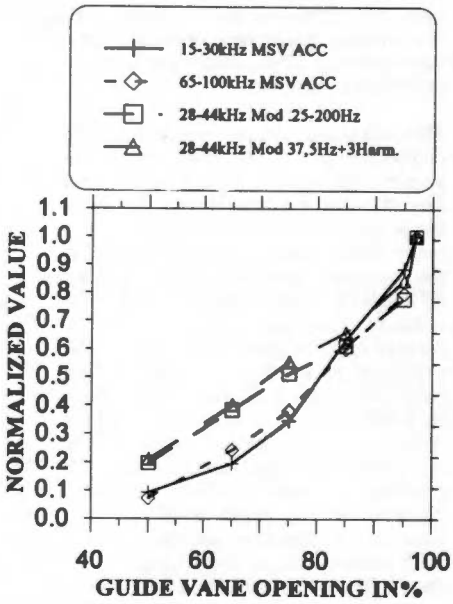

Fig.16. Vibratory cavitation signature of prototype B with leading edge cavitation damage.

important modulation components occurred at the guide vane passing frequency of 37.5 Hz and its next three harmonics, their contributions along with those of sidebands at +/- three times the rotation frequency were added together to form the curve with the triangles. Figure 16 is very representative of a leading edge cavitation problem which becomes very significant at the high flow velocities and alignment errors with the blades beyond the best efficiency point of the runner which in this case is located near 75% guide vane opening. All parameters follow the same typical trend at high guide vane opening since the leading edge impacts generally dominate all other signal components. Such is not the case in Figure 15 where the modulation of the high frequency acceleration at the guide vane passing frequency is completely out of phase with the three other parameters and reaches a peak value in the optimum operating range of the prototype.

The difference in the evolution of the modulation spectra of both machines with guide vane opening can be appreciated from Figures 17 and 18. Figure 17 pertains to the 240 MW prototype A with the trailing edge damage and Figure 18 to the 200 MW machine B with the leading edge problem. Figure 17 shows the initial run-up modulation spectra where the 60 Hz component is seen to rise and then subside as the guide vane opening varies

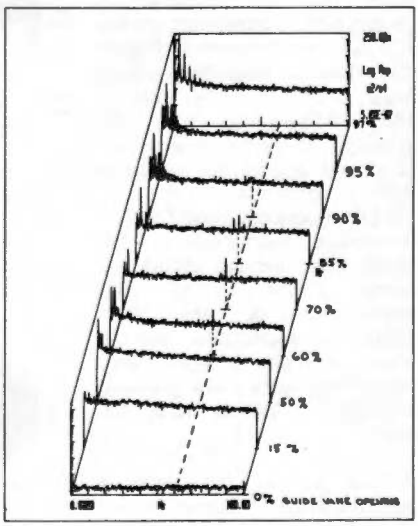

Fig. 17. Evolution of high frequency (70-85kHz) acceleration modulation autospectra during run-up in power on prototype A.

from 60 to 90%. Figure 18 for the leading edge cavitation case shows both the run-up and the run-down in guide vane opening. Here all components tend to increase with increasing guide vane opening. These data suggest that prototype A does not exhibit the traditional leading edge cavitation symptoms.

This becomes clearer still when the characteristics of the high frequency acceleration signal are examined in the time domain. Figures 19 and 20 show the acceleration signal recorded at the lower guide bearing of each machine in the upstream position with a Kistler 8616A1000 accelerometer during 0.75 rotation for machines A and B respectively. Figure 20 shows the typical large impacts of leading edge cavitation with a high crest factor (peak to RMS ratio). The modulation at the guide vane passing interval of 27 ms can even be detected easily. Figure 19 exhibits a signal with a different character as the peaks tend to have a more repetitive amplitude with consequently a lower crest factor. There also appear to be a multitude of smaller impacts with the 16 ms guide vane passing period apparent in the last half of the trace. These indications tend to confirm that we are confronted with outlet rather than inlet cavitation on prototype A. Further support for this hypothesis is seen in Figure 21 where a simplified sigma value expressed as the ratio of the submergence of the prototype to the headwater level is plotted against the measured MSV of acceleration in the 7 to 35 kHz frequency band for 219 11 minute observations at 77% guide vane opening during the winter months of 1993. The dependence of the high frequency acceleration on the value of sigma is very clear, suggesting again a low pressure cavitation situation near the outlet.

In addition to this data, a transmissibility function linking the damaged area on the blades to the monitoring point on the lower guide bearing had been averaged over the 13 blades. This function is illustrated in

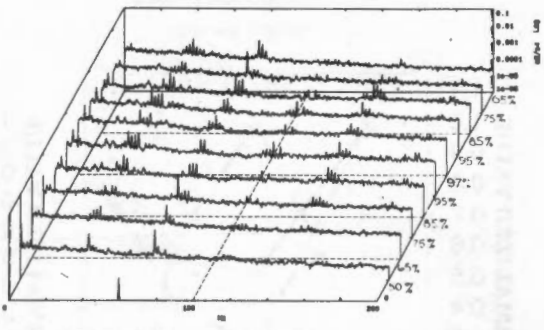

Fig. 18. Evolution of high frequency (28-44kHz) acceleration modulation autospectra during run-up and run-down in power on prototype B.

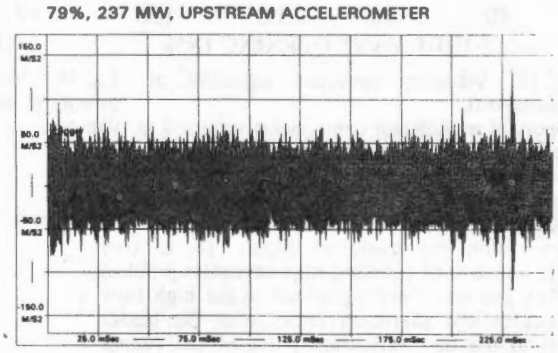

Fig. 19. Acceleration time trace for 0.75 revolution of prototype A at 237 MW.

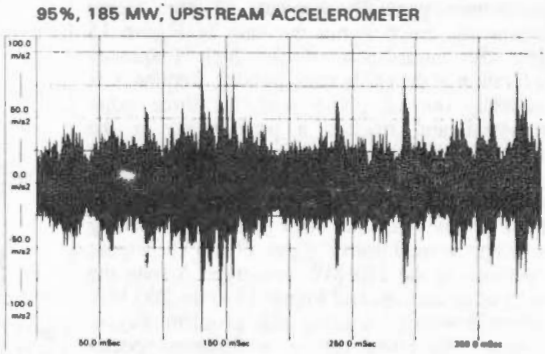

Fig. 20. Acceleration time trace for 0.75 revolution of prototype B at 185 MW.

Figure 22 along with the averaged coherence function. It indicates that the transmissibility function can only be used with confidence up to about 11 kHz to infer forces from measured acceleration autospectra under prototype operating conditions. These functions were however measured with the runner dewatered. Consequently, inferred forces will probably be underestimated as the transmissibility with the runner in water should be lower because of damping and loading effects of the water on the blade and crown vibrations. With all of this information in hand, it was decided to proceed to the pitting tests on the prototype, choosing in particular the test points in the area of the peak of the 60 Hz modulation component in Figures 15 and 17.

3.4 Pit counting tests on prototype A

3.4.1 Polished 316L sample installation. Optical quality polished 316L stainless steel disks were embedded flush with the profile of blade 4 of prototype A in the area were the cavitation erosion damage was most severe in the two observation periods up to 1990 and 1992 respectively. The 40 mm diameter disks were epoxy glued in counterbored recesses as shown on Figure 23 according to techniques in use at Électricité de France. Before each test, the glue was allowed to cure the required amount of time, then the access plank was removed, the machine watered , the necessary electrical security and start-up procedures executed and the test run for the planned exposure period. After a test, the reverse procedure was implemented to remove the exposed samples.

3.4.2 Prototype paint treatment. Prior to these tests the complete runner had been sandblasted and painted with an epoxy paint. This paint allowed to assess the aggressiveness of the cavitation on all the blades as it was eroded during the tests in those areas where the attack was most intense.

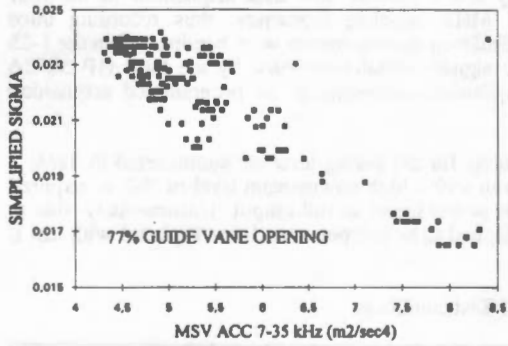

Fig. 21. Variation of high frequency acceleration with sigma on prototype A.

3.4.3 Vibratory sensors and data acquisition systems. For the purposes of the pitting tests, 2 new Endevco model 7259-25 accelerometers were installed at the upstream (0 degree) and 90 degree clockwise

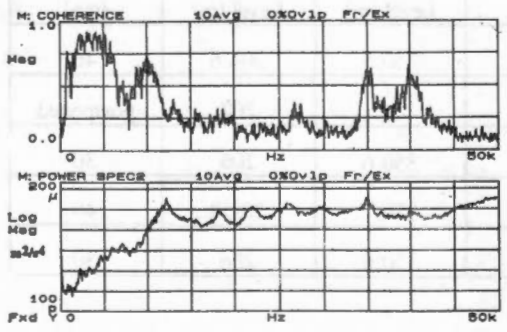

Fig. 22. Averaged Transmissibility function of prototype A.

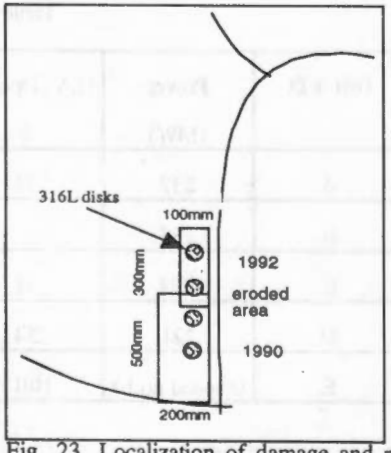

Fig. 23. Localization of damage and pit counting 316L disks on blade 4 of prototype A.

monitoring positions at the lower guide bearing as viewed from the alternator end of the shaft. A Kistler 8616A1000 accelerometer was added next to the 0 degree Endevco accelerometer so that cavitation impacts could be more easily identified by the excitation of the higher mounted resonance of this accelerometer (~115kHz in this case). A second Kistler accelerometer was mounted above the draft tube access door just a few centimeters below the lower level of the runner. This sensor was installed to appreciate the intensity of the mechanical excitation in this area, since damages on the runner had been found to be localized near the trailing edges of the blades during the first period of operation. An infrared tachometric probe detecting a rotating reflective target on the turbine shaft was also installed at the lower guide bearing to allow synchronized data acquisition. Data were acquired with a multichannel HP 3565S data acquisition system under control of LMS Fourier Monitor software, a Nicolet 500 four channel time data acquisition system with 12 bit 10 MHz A/D converters and 1 megasample memories on each channel and the local HP3852A cavitation monitoring system.

Data were acquired according to the following sequence: after machine stabilization, the simultaneous autopower spectra of the four accelerometers were measured in six lots of 30 averages in the 0-100 kHz frequency band. Each of the averages was obtained over a 8192 time sample acquisition on each sensor signal. The MSV of acceleration in the 15-30 and 65-100 kHz bands were then extracted. The high frequency acceleration envelopes were then recorded in the time domain in the form of 10 synchronized 8192 data points to allow subsequent frequency analysis in the 0-200 Hz frequency band. The envelope of the upstream 0 degree Endevco accelerometer bandpassed in the 15-30 kHz frequency band was first recorded, then that of the Kistler accelerometer at the same location bandpassed in the 65-100 kHz band and finally that of the Kistler accelerometer at the draft tube in the same manner. These acquisitions were then followed by a one second time data acquisition of the four sensors on the Nicolet system with a 1 MHz sampling frequency, thus recording three complete revolutions of the runner. The 2 Endevco accelerometers were bandpassed in the 1-25 kHz band for this purpose to simulate the signals actually recorded by the local HP 3852A monitoring system that completed the acquisitions according to its programmed acquisition cycles.

3.4.4 Test conditions. The test conditions for the pitting tests are summarized in Table 2 below. Test B which was scheduled to be run with a high downstream level of 207 m required the simultaneous operation of all units in the power house at full output. Unfortunately, due to network constraints, this important test point had to be postponed and was replaced with test E in the speed no load condition.

Table 2 Test conditions

Test I.D.	Power (MW)	G.V. Opening %	Upstream Level (m)	Downstream Level (m)	Duration (mn)
A	237	78	350.5	204.6	46
B	235			207	postponed
C	263	88	350.6	205	30
D	221	74	350.7	204.8	40
E	0(speed no l.)	10/15	350.6	206	30

3.4.5 Test results

3.4.5.1 Vibratory results. The main results of the vibratory measurements during the pitting tests are summarized in Figures 24, 25 and 26. The MSV of acceleration in the 15-30 kHz frequency band is seen to show little variation over the three test conditions with lower values recorded at the 237 MW point for all three guide bearing accelerometers. The draft tube accelerometer sees a dramatic increase in level at the high output power point as a result of much increased cavitation impacts visible in time recordings of the signal. The guide bearing accelerometers follow the trend visible in Figure 15 where little variation of this parameter was perceptible in the 74 to 88% range of guide vane opening utilized for the pitting tests. In Figure 25, the MSV of modulation components of the 0 degree Endevco and Kistler guide bearing accelerometers appear also to follow the original trend of the 60 Hz modulation component in Figure 15. A peak value is detected at the 237 MW point on both accelerometer signals. The draft tube accelerometer sees little modulation at these frequencies for the two lower power output conditions but goes to a maximum value at 263 MW output. As suggested by Figure 24, the cavitation activity appears to migrate towards the draft tube as power is increased.

Figure 26 presents the forces inferred on the blades from the acceleration autospectra of the 90 degree Endevco guide bearing accelerometer and the transmissibility function of Figure 22. Here also the high values are obtained at the two lower output power levels as inferred forces decrease at the 263 MW power point. By considering the typical damaged area of 300 cm^2 on a blade of the prototype and the per blade MSV of inferred force of 24 x 10^6 N^2, a data point was added to Figure 27 which summarizes past experience with vibratory cavitation set-ups, jet cavitation set-ups and Francis model, NACA profile in a cavitation tunnel and prototype of the model[10]. The observed averaged erosion rate of 8 mm/a of 308 stainless steel was converted by the factor of 2 to equivalent titanium grade 2 erosion rates for inclusion on the graph. This

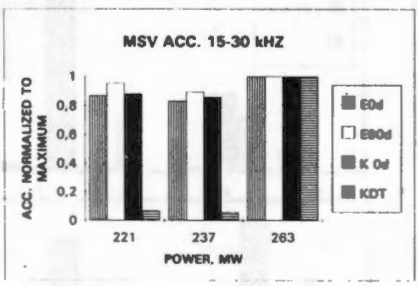

Fig. 24. Normalized MSV of 15-30kHz acceleration for the 4 accelerometers vs power output.

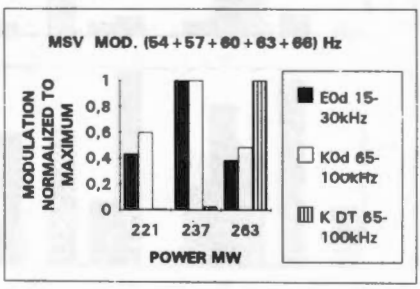

Fig. 25. Normalized MSV of high frequency acceleration modulation at 60 Hz +/- 1 and 2 times the rotation frequency.

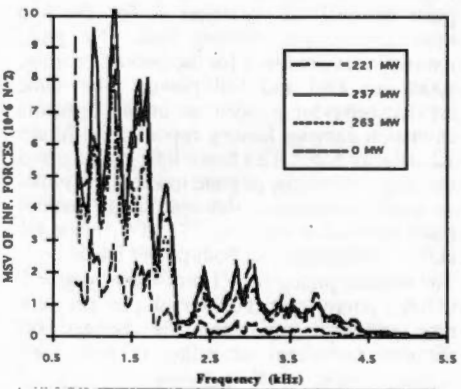

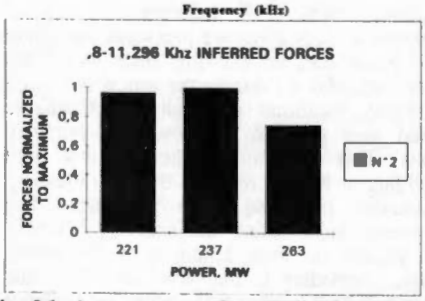

Fig. 26. Autospectra and normalized average values of MSV of inferred forces for the three test conditions of prototype A.

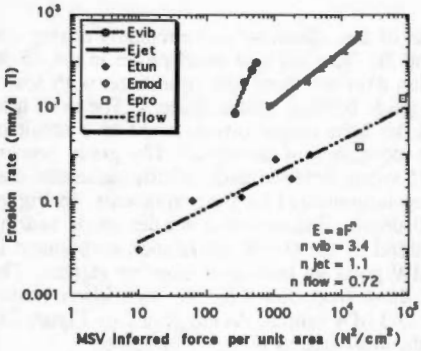

Figure 27. Correlation between erosion rate and inferred force per eroded unit area for vibratory, jet, tunnel, model and prototype Francis cavitation.

point fits well in the extension of the three preceding flow situations and indicates that the observed severe erosion rate is confirmed by the vibratory measurements.

3.4.5.2 Paint and pit counting results

Figure 28 presents the area and localization of paint removal on prototype A for the two most erosive pit counting tests. No paint removal was observed for the two other tests, speed no load and full power. The same erosive behavior is seen as in the previous cavitation damage history reported on figure 12. Blades 5,6,8,12 shows little erosion and the largest damages migrate towards the outlet as power increases. Although larger overall paint removal is seen for 237 MW, blade #4 shows similar area for both power levels.

The volume pitting rate (1 $mm^3/mm^2.year$ = 1 mm/a), pitting rate (number of pits per unit time and unit area) and the average pit diameter (weighted according to their total volume fraction)[12] measured on the 4 embedded 316l discs are presented on figure 29. Some data are missing since two discs were stripped off during the test at two high intensity locations although the technique used was proofed in previous laboratory tests. This corroborates the fact that only welding or bolting resist to the high intensity cavitation of these large machines. The highest volume pitting rate is seen at 221 MW on the disc the most distant from the trailing edge. According to the paint indication this disc was well located at the most intense spot at this power setting and this value should give a good estimation of the maximum

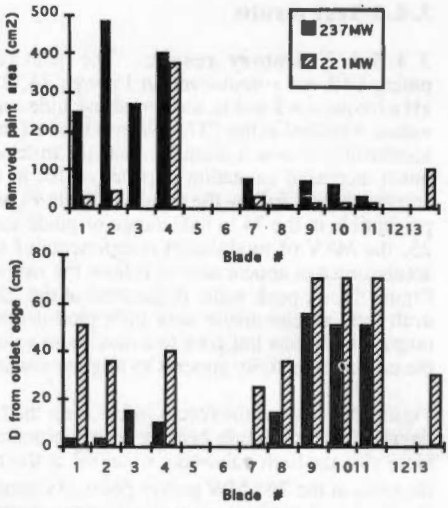

Figure 28. Area and localization of paint removal on proto. A for the two pitting tests.

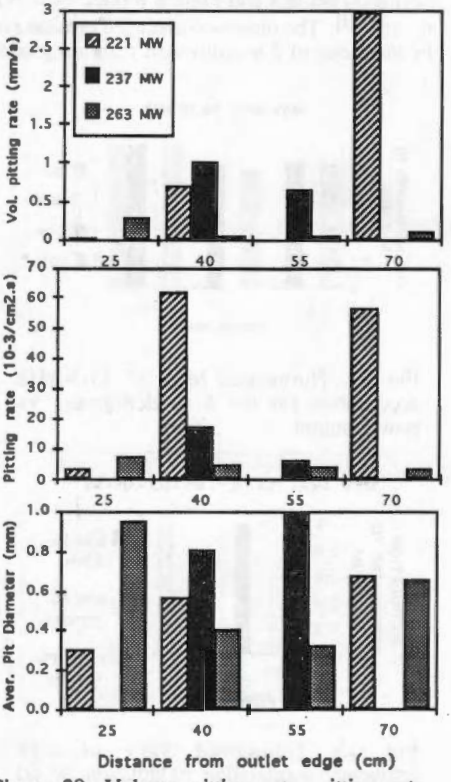

Figure 29. Volume pitting rate, pitting rate and aver. pit diameter measured on the 316L discs in the three tests of prototype A.

erosion rate at this power. At 237 MW the highest intensity spot was close to the disc stripped away, the closest to the trailing edge. As indicated by the pitting of the two other discs the cavitation intensity decreases towards upstream at this setting. The previous calibration in jet tests indicated that the volume pitting rate is about one half the penetration rate on 316L stainless steel. The maximum volume pitting rate value found of 3 mm per year would yield a penetration rate of about 6 mm/a of 316L, which is not far from the maximum erosion rate measured on the 308 overlay. The maximum pitting rate or repetition rate of the cavitation impacts measured at 221 MW of 60 x 10^{-3} per cm^2 per second would yield a total impact rate on the 300 cm^2 eroded area of the blade a little smaller than 60 per second which is the wicket gate passing frequency well detected by the vibratory technique. The average pit diameter are somewhat larger for the higher power 237 MW test, although less numerous.

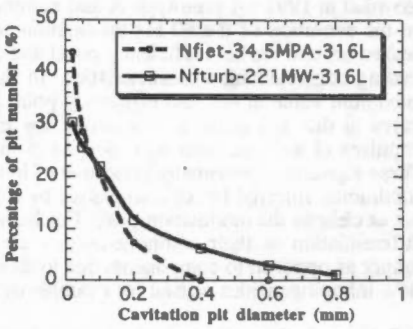

Fig. 30. Comparison of pit diameter on 316L in the highest intensity jet and on prototype A.

4 DISCUSSION

4.1 Jet and turbine pitting

Figures 30 and 31 show that the pit diameters observed on 316L samples on prototype A are substantially larger than those produced by the highest intensity of the cavitating jet. These results confirm that substantially bigger cavities are generated in water flow of larger machines. Material resistance to turbine cavitation should be evaluated with this in mind. Thus the jet at its highest intensity is the best presently acceptable simulator of turbine cavitation though its individual impacts are still unable to reproduce the craters found in short term cavitation exposure at the prototype level.

4.2 Vibratory measurements

The choice of the test points for these pitting tests was made from the cavitation signatures

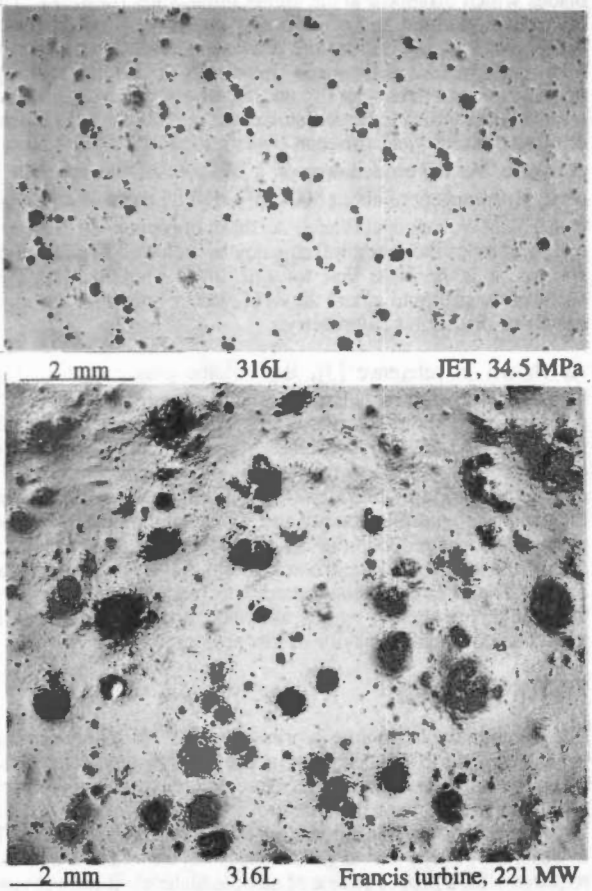

Fig. 31. Optical micrographs of cavitation pits on 316L in the highest intensity jet (0.15s) and on prototype A (40min) at 221 MW.

recorded in 1991 on prototype A and summarized in Figure 15. They were based particularly on the evolution of the 60 Hz modulation component of the high frequency vibration which peaked around the best efficiency point and time data recordings which did not exhibit typical leading edge cavitation characteristics. In the pitting tests this component again passes by a maximum value at the best efficiency point as shown in Figure 25. The examination of time traces at this test point also revealed the existence of clusters of numerous tightly spaced impulses (1 to 2 ms spacing) modulated in amplitude at the guide vane passing frequency. These signals are potentially indicative of bubble cavitation initiated by mid-blade low pressure conditions. Inferred forces also passed by a peak at the best efficiency point but this peak was not as clear as the modulation peak. For both of these parameters, the real challenge lies in the differentiation of their components that are exclusively linked to cavitation impacts on the runner as opposed to components due to flow noise or harmonic pressure pulsations caused by flow inhomogeneities caused for example by guide vane perturbations.

4.3 Correlation of pit counting, paint erosion and vibratory detection

The 60 Hz modulation component could well be indicative of the cavitation impacts on the blades which disappear at the higher guide vane openings. The hypothesis of the stretching of the cavitation cloud and of its implosion in the flow downstream of the blade trailing edge at full power is supported by the marked increase of the vibration modulation seen by the draft tube accelerometer at the same frequency, 60 Hz, as the impacts on the blades at the lower output test conditions (see Figure 25). These vibratory measurements also agree with the paint removal data which indicate that the test at 237 MW was the most erosive. An impact frequency of 60/sec would yield for each blade a total of 40X60X60 = 144000 impacts for a 40 minute exposure. As the eroded area on a blade is of the order of 300 cm^2 , we should achieve a density of impacts of about 500/cm^2, slightly more than the maximum density observed in test D at 221 MW, that is 100/cm^2. As these impacts at 60 Hz are themselves strongly modulated at once and twice the rotation frequency as indicated by sidebands about 60 Hz in the modulation spectra, it is possible that for one blade in particular, the most violent implosions, i.e. sufficiently strong to indent the 316L, occur only over a portion of a revolution as a result of a runner or distributor asymmetry.

As shown in reference [3], the volume pitting rate of 316L is equal to about twice its penetration erosion rate. Thus a volume pitting rate of 30 $X10^{-3}$ $mm^3/h.cm^2$ is equivalent to an erosion rate of about 6 mm/a, which is of the same order of magnitude as the maximum erosion rates observed on this prototype. Moreover, the localization of the more severe and closer to the trailing edge erosion of the first observation period, 89-90 during which the unit was operated for a long while at 240 MW, supports also this model of cavitation demeanor. As all the paint removal, pit counting and vibratory modulation measurements have indicated in these pitting tests, the reduction of the average output power from 231 to 215 MW had for effect to reduce the intensity of the erosion and to displace it upstream away from the trailing edge of the blades. The three cavitation detection techniques applied in these tests have allowed to develop through their coherent results and their complementariness a plausible understanding of the particular cavitation behavior of this prototype.

5 CONCLUSIONS

The pit counting technique works very well in laboratory cavitation set-ups and has shown itself adaptable to field measurements on prototype runners and in so doing has by the same token demonstrated the impressive aggressiveness of prototype cavitating flow. Strong attachment methods of the samples are required, particularly if the technique is to be used for the potentially more violent leading edge cavitation appraisal. This technique is an excellent tool to describe directly the aggressiveness of the erosive power of a flow. It is as sensitive as required with a proper choice of sample material, it can provide quantitative results with a laser profilometer and it is directly related to the erosion rate measured by weight loss. It is complemented by the paint removal assessment which allows to locate the samples correctly and to obtain a global erosion picture of the prototype.

The vibratory technique with a high frequency accelerometer has shown itself very promising. It is the most sensitive as it can identify the level of attack well before pits or erosion occur. It is also instantaneous and allows a global measure of the effects of the complete cavitation phenomena. However, even if the MSV of acceleration or inferred forces have shown excellent correlations in the jet tests, measurements on the prototype have shown that a simple universal relation to quantify erosion with this technique was not yet available. While applications with leading edge cavitation where the strong impacts tend to dominate the vibration signal appear more straightforward to analyze, cases such as the one experienced with this prototype where low pressure mid-blade bubble cavitation is probably present require the use of many criteria in the analysis of the vibratory signal to quantify cavitation erosion or the potential erosive power[13]. In all cases, the impulsive components of the vibratory response due to cavitation must be identified separately from the contributions of flow noise, non damaging cavitation in the flow and harmonic hydrodynamic forces acting at the impact frequencies. The present results indicate that it is possible to obtain a quantitative relation with erosion rate by the selection of the proper frequency bandwidth and modulation.

Both vibratory and pit counting techniques have been found quantifiable and sensitive enough to detect the very low cavitation intensity observed in model tests of Francis turbines. They should be very useful in establishing the scaling laws between model and prototype cavitation erosion in Francis turbines.

6 ACKNOWLEDGMENTS

The authors would like to thank Hydro-Québec Électricité de France and EPFL-IMHEF of Lausanne for making these research efforts possible. Special thanks go to the crew at the Hydro-Québec powerplant where the pitting tests were performed, to Philippe Behar of EDF for the pitting tests, Jacques Larouche of IREQ who performed the jet tests and Pierre Lavigne also of IREQ for his involvement in the vibratory aspect of the jet and prototype tests.

REFERENCES

1 Simoneau, R., Pétrin, M.-C., "Cavitation damages of hydraulic turbines", Cavitation Erosion of Hydraulic Turbines CEA Workshop, Montréal, Vancouver, March 1994.

2 Laperrousaz, E., Dorey, J.M., Rigg, J.P., Simoneau, R., Avellan, F., Henry, P., "Predicting cavitation in Francis turbines on the basis of scale model testing", 17th AIRH Symposium, Beijing, September 1994.

3 Simoneau, R., Bourdon, P., Farhat, M., Avellan, F., Dorey, J.M., "Cavitation erosion, impact intensity and pit size distribution of jet and vortex cavitation", Bubble Noise and Cavitation Erosion in Fluid Systems, ASME annual winter meeting, New Orleans, December 1993.

4 Bourdon, P., Simoneau, R., Lavigne, P., "A vibratory approach to the detection of erosive cavitation", Proc. of Third International Symposium on Cavitation Noise and Erosion in Fluid System, ASME, San Francisco (USA), December 1989.

5 Bourdon, Paul, Simoneau, R., Avellan, F., "Erosion vibratory fingerprint of leading edge cavitation of a NACA profile and a Francis model and prototype hydroturbine", ASME Bubble Noise and Cavitation Erosion Symposium, New-Orleans, December 1993.

6 Abbot, P.A., "Cavitation detection measurements on Francis and Kaplan Hydroturbines", Proc. of Third International Symposium on Cavitation Noise and Erosion in Fluid System, ASME, San Francisco (USA), December 1989.

7 Lecoffre, Y., Marcoz, J., Franc, J. P., Michel, J. M., "Tentative procedure for scaling cavitation damage", Intern. Sympos. on Cavitation in Hydraulic Structure and Turbomachinery, ASME, Albuquerque, June 1985.

8 Dorey, J.M., Le, Q., Tura, F., "A new test procedure using paint and polished samples to quantify cavitation agressivity on industrial components", ASME Cavitation '91, Portland, Oregon, June 1991.

9 Simoneau, R., "Vibratory, jet and hydroturbine cavitation erosion", Cavitation and Multiphase Flow Forum, ASME-JSME Fluids Eng. Conf., Portland, Oregon, June 1991.

10 Simoneau, R., Bourdon, P., "Erosion and impact intensity of vibratory, jet and turbine cavitation", 16th IAHR Symposium, Sao Paolo, Brazil, September 1992.

11 Bourdon, P., Simoneau, R., Avellan, F., "Hydraulic turbine cavitation pitting detection by monitoring runner vibration", CEA final project report 307 G 657, Montréal, June 1993.

12 Dorey, J.M., Simoneau, R., Bourdon, P., Farhat, M., Avellan, F., "Quantification of cavitation aggressiveness in three different devices using accelerometer, DECER and pitting measurements", The Second International Symposium on Cavitation, Tokyo, April 1994.

13 Avellan, F., Dupont, Ph., Farhat, M., "Cavitation erosion power", ASME Cavitation '91, Portland, Oregon, June 1991.